NASA/TM—2015-218748

A Fully Nonmetallic Gas Turbine Engine Enabled by Additive Manufacturing

Part I: System Analysis, Component Identification, Additive Manufacturing, and Testing of Polymer Composites

Joseph E. Grady, William J. Haller, Philip E. Poinsatte, Michael C. Halbig, and Sydney L. Schnulo
Glenn Research Center, Cleveland, Ohio

Mrityunjay Singh
Ohio Aerospace Institute, Brook Park, Ohio

Don Weir, Natalie Wali, and Michael Vinup
Honeywell Aerospace, Phoenix, Arizona

Michael G. Jones
Langley Research Center, Hampton, Virginia

Clark Patterson and Tom Santelle
Rapid Prototyping+Manufacturing (rp+m), Avon Lake, Ohio

Jeremy Mehl
Princeton University, Princeton, New Jersey

May 2015

NASA STI Program . . . in Profile

Since its founding, NASA has been dedicated to the advancement of aeronautics and space science. The NASA Scientific and Technical Information (STI) Program plays a key part in helping NASA maintain this important role.

The NASA STI Program operates under the auspices of the Agency Chief Information Officer. It collects, organizes, provides for archiving, and disseminates NASA's STI. The NASA STI Program provides access to the NASA Technical Report Server—Registered (NTRS Reg) and NASA Technical Report Server—Public (NTRS) thus providing one of the largest collections of aeronautical and space science STI in the world. Results are published in both non-NASA channels and by NASA in the NASA STI Report Series, which includes the following report types:

- TECHNICAL PUBLICATION. Reports of completed research or a major significant phase of research that present the results of NASA programs and include extensive data or theoretical analysis. Includes compilations of significant scientific and technical data and information deemed to be of continuing reference value. NASA counter-part of peer-reviewed formal professional papers, but has less stringent limitations on manuscript length and extent of graphic presentations.

- TECHNICAL MEMORANDUM. Scientific and technical findings that are preliminary or of specialized interest, e.g., "quick-release" reports, working papers, and bibliographies that contain minimal annotation. Does not contain extensive analysis.

- CONTRACTOR REPORT. Scientific and technical findings by NASA-sponsored contractors and grantees.

- CONFERENCE PUBLICATION. Collected papers from scientific and technical conferences, symposia, seminars, or other meetings sponsored or co-sponsored by NASA.

- SPECIAL PUBLICATION. Scientific, technical, or historical information from NASA programs, projects, and missions, often concerned with subjects having substantial public interest.

- TECHNICAL TRANSLATION. English-language translations of foreign scientific and technical material pertinent to NASA's mission.

For more information about the NASA STI program, see the following:

- Access the NASA STI program home page at http://www.sti.nasa.gov

- E-mail your question to help@sti.nasa.gov

- Fax your question to the NASA STI Information Desk at 757-864-6500

- Telephone the NASA STI Information Desk at 757-864-9658

- Write to:
  NASA STI Program
  Mail Stop 148
  NASA Langley Research Center
  Hampton, VA 23681-2199

NASA/TM—2015-218748

A Fully Nonmetallic Gas Turbine Engine Enabled by Additive Manufacturing

Part I: System Analysis, Component Identification, Additive Manufacturing, and Testing of Polymer Composites

Joseph E. Grady, William J. Haller, Philip E. Poinsatte, Michael C. Halbig, and Sydney L. Schnulo
Glenn Research Center, Cleveland, Ohio

Mrityunjay Singh
Ohio Aerospace Institute, Brook Park, Ohio

Don Weir, Natalie Wali, and Michael Vinup
Honeywell Aerospace, Phoenix, Arizona

Michael G. Jones
Langley Research Center, Hampton, Virginia

Clark Patterson and Tom Santelle
Rapid Prototyping+Manufacturing (rp+m), Avon Lake, Ohio

Jeremy Mehl
Princeton University, Princeton, New Jersey

National Aeronautics and
Space Administration

Glenn Research Center
Cleveland, Ohio 44135

May 2015

Acknowledgments

The authors would like to thank Drs. Mike Dudley and Koushik Datta from NASA Aeronautics Research Institute for their continuous support and encouragements. We would like to thank test facility staff at NASA Glenn Research Center and NASA Langley Research Center for their help in IGVs and acoustic liner testing. The authors would also like to recognize Jeff Berton, Scott Jones and Mike Tong from the propulsion systems analysis organization at NASA Glenn Research Center who provided key technical support during the benefit assessment effort. Technical help from various engineers from Honeywell and rp+m during this work is also gratefully acknowledged.

Level of Review: This material has been technically reviewed by technical management.

Available from

NASA STI Program
Mail Stop 148
NASA Langley Research Center
Hampton, VA 23681-2199

National Technical Information Service
5285 Port Royal Road
Springfield, VA 22161
703-605-6000

This report is available in electronic form at http://www.sti.nasa.gov/ and http://ntrs.nasa.gov/

A Fully Nonmetallic Gas Turbine Engine Enabled by Additive Manufacturing
Part I: System Analysis, Component Identification, Additive Manufacturing, and Testing of Polymer Composites

Joseph E. Grady, William J. Haller, Philip E. Poinsatte, Michael C. Halbig, and Sydney L. Schnulo
National Aeronautics and Space Administration
Glenn Research Center
Cleveland, Ohio 44135

Mrityunjay Singh
Ohio Aerospace Institute
Brook Park, Ohio 44142

Don Weir, Natalie Wali, and Michael Vinup
Honeywell Aerospace
Phoenix, Arizona 85034

Michael G. Jones
National Aeronautics and Space Administration
Langley Research Center
Hampton, Virginia 23681

Clark Patterson and Tom Santelle
Rapid Prototyping+Manufacturing (rp+m)
Avon Lake, Ohio 44012

Jeremy Mehl
Princeton University
Princeton, New Jersey 08544

Abstract

The research and development activities reported in this publication were carried out under NASA Aeronautics Research Institute (NARI) funded project entitled "A Fully Nonmetallic Gas Turbine Engine Enabled by Additive Manufacturing." The objective of the project was to conduct evaluation of emerging materials and manufacturing technologies that will enable fully nonmetallic gas turbine engines. The results of the activities are described in three part report. The first part of the report contains the data and analysis of engine system trade studies, which were carried out to estimate reduction in engine emissions and fuel burn enabled due to advanced materials and manufacturing processes. A number of key engine components were identified in which advanced materials and additive manufacturing processes would provide the most significant benefits to engine operation. The technical scope of activities included an assessment of the feasibility of using additive manufacturing technologies to fabricate gas turbine engine components from polymer and ceramic matrix composites, which were accomplished by fabricating prototype engine components and testing them in simulated engine operating conditions. The manufacturing process parameters were developed and optimized for polymer and ceramic composites (described in detail in the second and third part of the report). A number of prototype components (inlet guide vane (IGV), acoustic liners, engine access door) were additively manufactured using high

temperature polymer materials. Ceramic matrix composite components included turbine nozzle components. In addition, IGVs and acoustic liners were tested in simulated engine conditions in test rigs. The test results are reported and discussed in detail.

Introduction

Advanced lightweight and high temperature materials and technologies have made tremendous impact on the aerospace components and systems in terms of weight reduction, high operating temperature, reduced fuel burn, and reduced emissions. In particular, advances in composites materials and manufacturing technologies enabled the first polymer matrix composite (PMC) fan blades and fan containment system in gas turbine engines in the 1990s. More recent advances in ceramics and coatings will soon enable the first ceramic matrix composite (CMC) components in commercial aircraft engines in 2016. Recent high TRL demonstration of CMC exhaust nozzle components will lead to introduction of CMC exhaust nozzles in commercial engines in the near future. Even with the introduction of PMCs and CMCs in gas turbine engines, the percentage of composites in these engines is relatively small, on the order of 10 to 20 percent, compared to nearly 50 percent for airframe structures, with most of it consisting of metallic components.

As the temperature capability of PMCs increase from the state of the art (SOA) of 150 °C (300 °F) to 350 °C (660 °F), the PMCs can be applied for a wide range of gas turbine structures. Similarly, the CMC technology continues to advance (Ref. 1). Advanced composite materials have created new opportunities for innovative component designs and new gas turbine designs/architectures that can take full advantage of the properties of the unique properties of composites. A wide variety of metallic components in the hot sections of current gas turbine engines could be replaced with ceramic matrix composites, reducing engine weight and the need for cooling air, and therefore increasing engine efficiency and reducing emissions and fuel burn.

The goal of the current project, funded by NASA Aeronautics Research Institute (NARI), was to perform comprehensive evaluation of emerging materials and manufacturing technologies that will enable fully nonmetallic gas turbine engines. The technical activities were carried out to assess the feasibility of additive manufacturing technologies for fabricating complex polymer matrix composite (PMC) and ceramic matrix composite (CMC) gas turbine engine components. System analysis studies were conducted to assess the benefits of fully nonmetallic gas turbine engine in terms of fuel burn, emissions, reduction of part count, and cost. The potential benefits of this effort include:

- Significant reduction in number of heavy metallic components, with more than 50 percent reduction of weight and the associated reduction of fuel burn/carbon dioxide emissions
- Reduction in manufacturing costs by the simplified additive manufacturing of composite
- Structural components, replacing casting of metals
- Engine weight and part count reduction by reducing the need for joining and attachment of components
- New engine architectures enabled by the unique properties of composites

However, comprehensive engine design studies needs to be conducted to develop design and architecture concepts for a fully nonmetallic gas turbine engine that can be enabled by effective use of PMCs, CMCs and ceramic materials and integration of components through additive manufacturing of complex components.

In order to demonstrate this concept, the effort was focused on 7000 lbf gas turbine engine. However, the materials and manufacturing technologies developed in this program are equally applicable to large gas turbine engine. The technical work was carried out by multidisciplinary, multiorganization NASA—industry team that included experts in engine design and analysis, and system analysis, additive manufacturing, polymers and PMCs, structural engineering, ceramic materials and CMCs, and sub-component testing under simulated engine conditions.

System Analysis and Potential Benefits

The systems analysis effort was tasked with evaluating the potential fuel burn, landing-takeoff (LTO) NO_X and acoustic benefits of polymer matrix and ceramic matrix composite materials in a regional jet class engine. The first step in the process was the development of the current technology, small thrust (i.e., regional jet class) engine to serve as the baseline. After investigating the potential engine options and interaction with Honeywell, the initial decision was for the NASA systems analysis team to use an "AE3007-like" engine. The process began with a review of the existing Numerical Propulsion System Simulation (NPSS) engine model (Refs. 2 to 4) and several issues were discovered. The model was constructed several years ago and needed significant updating to work with the current version of NPSS. The team then decided that an alternate engine cycle was needed. The systems analysis organization had a functioning NPSS model of a CF34-8C "like" engine, along with an airplane model of the CRJ-900 regional jet that uses the CF34 engine. Both models were created by Georgia Tech during the development of the FAA-sponsored Environmental Design Space (EDS capability) (Ref. 5). A key part of the EDS development process involved industry feedback on the model assumptions. Although the CF34-8C is a larger thrust engine than the AE3007, it does reside in the regional jet thrust class. After consultation with the other team members, and with Honeywell's concurrence, the decision was made to proceed with the CF34-8C as the baseline. Figure 1 shows the baseline engine and airplane data used for the system analysis of engine (CF34-8C5 "like") and the airframe (CRJ900LR "like").

	Aero Design Point (M0.80,35 kft)	Rolling Takeoff (M0.25, SL)	Sea Level Static (M0.0, SL)
Delta T (deg R)	0	+27	+27
F_N (lbf)	3510	12400	14505
BPR	5.13	5.15	5.11
OPR	27.5	24.0	23.3
T4 (deg R)	2840	3170	3100
T41 (deg R)	2680	3000	2935
SFC	0.6900	0.5269	0.4105

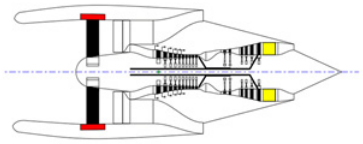

Weights		Dimensions	
Bare Engine Wt.	2505	Engine Length	93.6
Accessories Wt.	700	Engine Pod C. G.	32.5
Engine Wt.	3205	Engine Max. Diameter	47.5
Inlet/Nacelle Wt.	555	Nacelle Max. Diameter	62.3
Total Pod Wt.	3760	Total Pod Length	127.1

Gross Weight (lb):	84,500
Weight empty (lb):	44,200
Operating empty weight (lb):	47,200
Mission Fuel (lb):	19,670
Block Fuel (lb):	15,730
Block Time (min):	284
SLS Thrust per engine (lb_f):	14,500
Part 25 field length (ft):	6000
Cruise Mach/ICA (ft):	0.8, 35000

Design mission: Maximum takeoff gross weight mission with full passenger load (86 passengers) and fuel tanks completely filled. These requirements produce a design range 1980 nm.

Figure 1.—Key baseline engine and airplane data with design mission for current technology engine (CF34-8C5 "like") and the airframe (CRJ900LR "like").

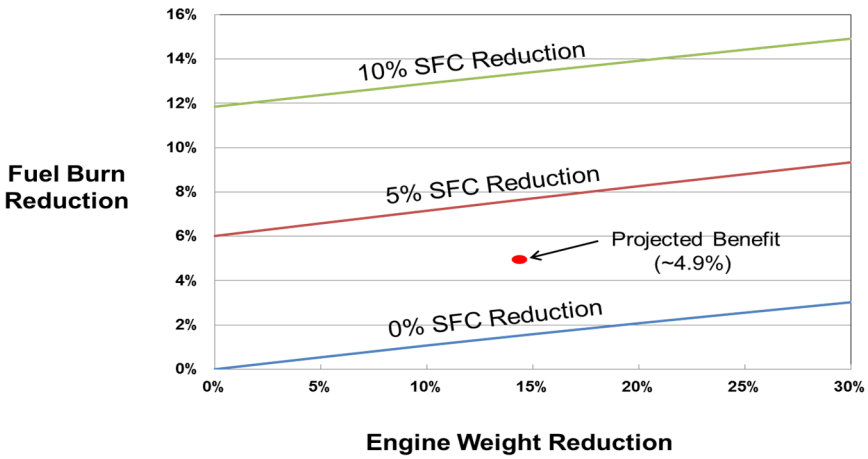

Figure 2.—Regional jet fuel burn sensitivities showing fuel burn reduction and engine weight reduction.

The analysis effort commenced with the generation of initial performance and weight benefits from inserting polymer matrix composites (PMC) and ceramic matrix composites (CMC) into the baseline engine. Based on input from the materials experts, it was decided that the maximum allowable material temperature for the PMCs was 415 °F). As such, PMCs were envisioned for use in several locations in the front portion of the engine (inlet acoustic duct, fan stator, and the first four rows of high-pressure compressor vanes). In the engine's hot section, 2600 °F CMCs were inserted in the combustor liner, high-pressure turbine (HPT) vanes/blades, low-pressure turbine (LPT) vanes/blades and core nozzle. The cycle was reoptimized to eliminate all turbine blade/vane cooling. The "advanced" cycle produced ~2.6 percent improvement in specific fuel consumption. The inclusion of the composite materials enabled the engine weight to decrease by ~14.5 percent. Figure 2 shows the analysis of regional jet fuel burn sensitivities indicating influence of engine weight reduction on the reduction in fuel burn. The combination of fuel efficiency improvement and engine weight reduction would indicate an airplane that has a 4.9 percent reduction in total fuel burn versus the current technology baseline.

The LTO NO_X benefit was derived primarily from the drop in combustor exit temperature with the addition of the uncooled, CMC turbine vanes and blades. The baseline engine had a margin to the CAEP/6 stringency of 20.4 percent. The "advanced" engine has a margin of 28.7 percent, an 8.3 percent increase. There were no direct acoustic benefits identified for the PMC and CMC materials. There was no change in the fan tip speed and minimal differences in the jet velocity versus the baseline engine. As such, it was determined that the "advanced" engine/airplane noise would be almost identical to the baseline. However, during the evaluation a potential noise reduction opportunity was discussed. Taking advantage of additive manufacturing could enable the production of variable depth inlet acoustic liners. This tailored approach could capture the larger tones and discrete frequencies and as such would provide an acoustic benefit. NASA acoustic discipline experts, in consultation with Honeywell, plan to work with the systems analysis team to develop a benefit from such a design. If the benefits can be quantified, a full system acoustic assessment could be conducted.

The second part of the assessment was to allocate the projected 4.9 percent fuel burn benefit between the PMCs and CMCs. Table 1 shows the influence of different materials and components on the system level benefits. In addition to the weight reduction versus the metallic parts replaced, CMC usage enabled the elimination of all turbine blade and vane cooling. By removing the need for cooling and the associated mixing losses, an efficiency improvement in the HPT (1.5 pts) and LPT (0.5 pt) was assumed. The PMC benefits were entirely weight reduction based and had no impact on the engine performance. As such, the vast majority (~90 percent) of the fuel burn improvement is attributed to the hot section CMCs.

TABLE 1.—EFFECT OF KEY MATERIALS TECHNOLOGIES ON VARIOUS SYSTEM LEVEL BENEFITS

	Baseline	Advanced (All Techs)	Advanced (PMCs only)	Advanced (CMCs only)
SFC (cruise)	0.6900	0.6719 (-2.6%)	0.6900	0.6719 (-2.6%)
SFC (SLS)	0.4105	0.3902 (-4.95%)	0.4105	0.3902 (-4.95%)
Engine Weight (lb)	3760	3215 (-14.5%)	3600 (-4.3%)	3375 (-10.2%)
Aircraft Weight (lb)	84500	81970 (-3.0%)	83965 (-0.7%)	82540 (-2.3%)
Block Fuel (lb)	15730	14960 (-4.9%)	15660 (-0.5%)	15040 (-4.4%)

In summary, an assessment was performed by NASA's propulsion systems analysis branch to quantify the potential benefits of PMC and CMC engine components that could be produced via additive manufacturing processes for a regional-jet class system. The study assumed the availability of 2600 °F CMCs and 415 °F PMCs. The CMCs were applied in the combustor liner, the high-pressure and low-pressure turbine blade/vanes and the core nozzle. The benefits included a weight reduction in the aforementioned components due to replacing metallic parts with ceramic-based alternatives, in addition to the elimination of requisite turbine cooling. The PMCs were applied in the inlet acoustic liner, the fan stator and the first four rows of the high-pressure compressor vanes. The PMC benefits consisted of weight reductions only in each component. The resultant propulsion system generated a 4.9 percent fuel burn improvement over the baseline and a 7.7 percent increase in landing-takeoff (LTO NO_X) margin with respect to the CAEP/6 stringency. The assessment estimated minimal acoustic impact. Finally, there may be some durability concerns with the use of composites in the turbine rotors and the fan stator that could merit further investigation.

Identification of Potential Components

Polymer Matrix Composites

During the initial phases of the project, several target components for the PMC manufacturing efforts were identified. These selections were made based on the operational requirements, material properties, manufacturing capability of commercially available and developmental polymer composites. The initial component list was narrowed to two types of components for the Phase I demonstration. Figure 3 shows few of the high-payoff engine components identified for advanced materials and manufacturing technologies Polymer based components included inlet guide vanes (IGVs) and acoustic liners. The inlet guide vane (IGV) is a static structural component currently made of Ti-6Al-4V alloy. This component is subjected to low pressures and temperatures suitable for the polymer matrix composite material systems assessed in this program. There has been industrial experience with manufacturing and testing a PEEK thermoplastic IGV. The polymer composite IGV components are expected to provide benefits from effective weight reduction, superior strength and temperature capability as well as advanced manufacturing processes of this program.

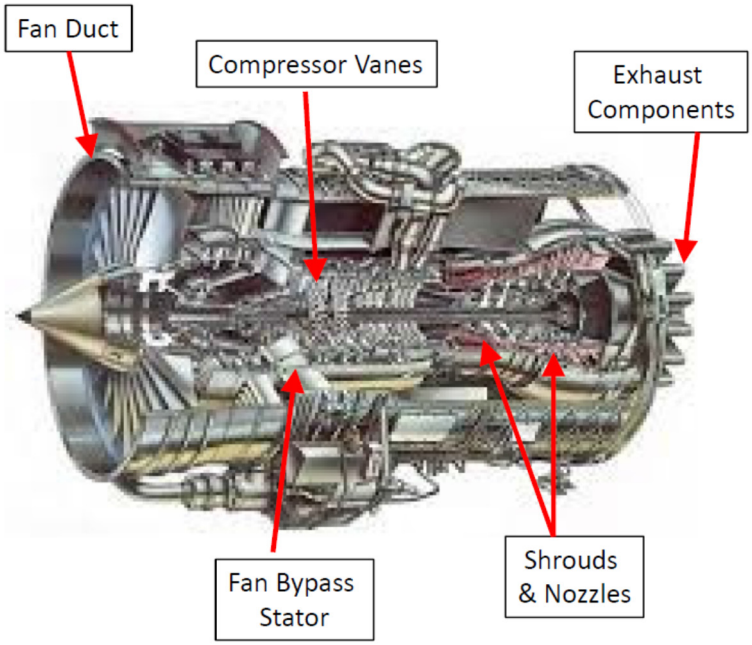

Figure 3.—High-payoff engine components identified for advanced materials and manufacturing technologies.

Acoustic attenuation materials are used in almost all components of a turbofan engine. Acoustic liner operating temperature is 250 °F for a typical propulsion engine aft-fan duct. Additive manufacturing may be used to make absorptive structures not feasible with conventional techniques. Previous efforts have been focused on locally-reacting resonator liners. This project will help to determine if it is possible to build advanced liners using passive-destructive interference or direct dissipation of the acoustic waves.

Traditional manufacturing methods typically used to fabricate locally-reacting resonator acoustic liners include fabrication of honeycomb resonator structures using sheet metal forming methods, fabrication of a porous facesheet using ultrasonic or laser drilling methods to form perforations in a sheet metal cover, and bonding facesheet to the honeycomb or bulk absorber using well known metal brazing or welding methods. Additive manufacturing processes combine all of these steps into a single process in which the component is fabricated by progressively building the structural element layer by layer, in a process driven by a geometric file describing the dimensions of the structure. Acoustic liner fabrication using traditional and an additive manufacturing approach is shown in Figure 4. No joining is needed and the required porosity is “built-in” to the facesheet without any need for post-fabrication drilling or machining. Novel acoustic liner concepts may also be constructed. This process has the added potential for reduced weight and fabrication cost.

The technical approach for evaluation of PMC acoustic liners fabricated by Fused Deposition Modeling included:

- Selection of a conventional liner sample from a previous NASA program (Ref. 6).
- Fabrication of a conventional locally reacting liner sample using additive manufacturing.
- Build and test the advanced liner concept shown in Figure 5, which is not feasible with conventional manufacturing techniques, using Fused Deposition Modeling.
- Test three samples in the NASA Langley Grazing Flow Impedance Tube (GFIT) shown in Figure 5.
- Fabricate a typical acoustically-treated access panel for a turbofan engine bypass duct.

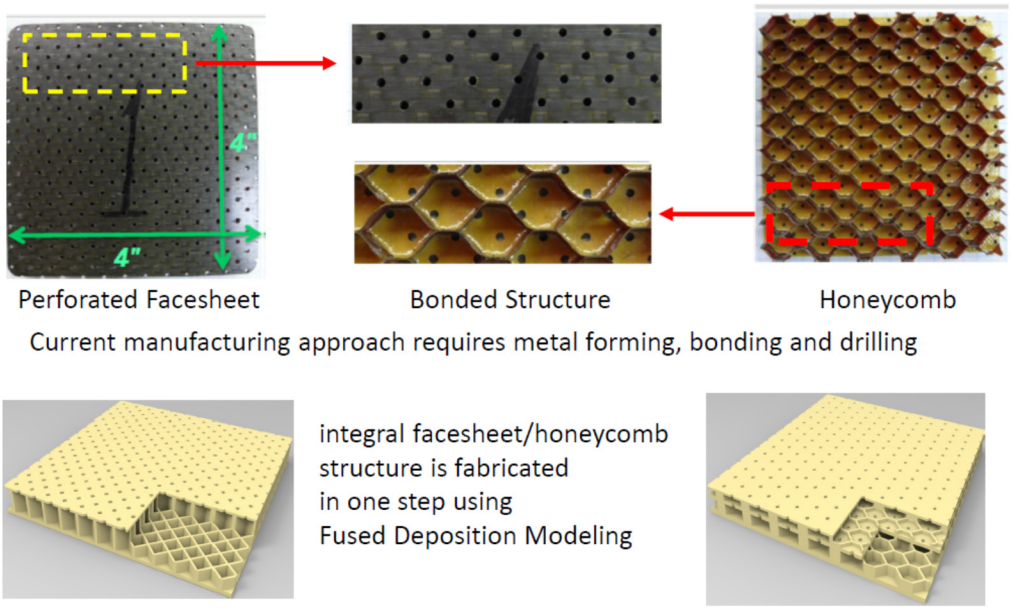

Figure 4.—Additive manufacturing simplifies acoustic liner fabrication.

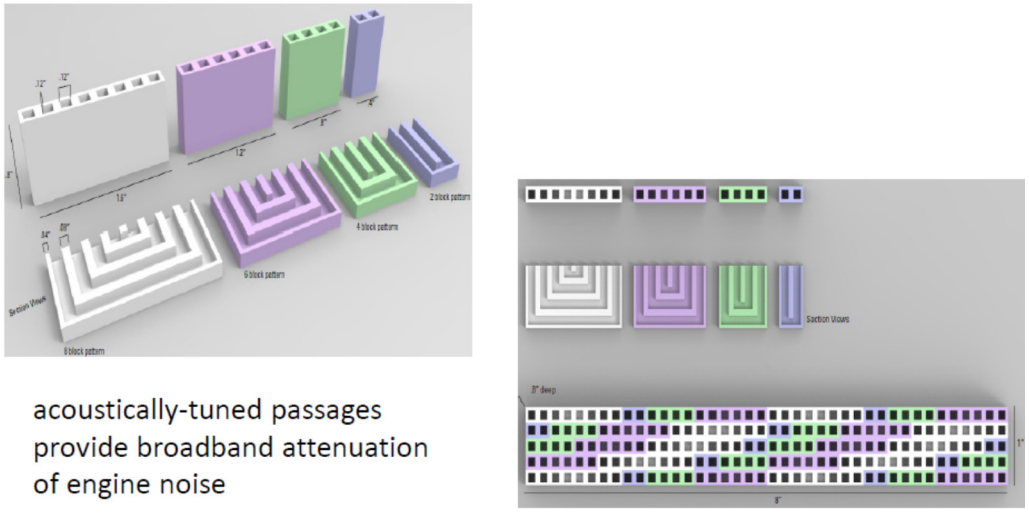

Figure 5.—Fused deposition modeling enables fabrication of advanced passive-destructive acoustic liner concept.

Ceramic Matrix Composites

A number of components were identified for the Phase I ceramic manufacturing effort. A balance had to be struck between identifying the components that would offer nontrivial fuel burn reduction if manufactured as ceramics and identifying the components that were relatively low-stress. Other factors included manufacturing complexity (e.g., geometry and cooling passage schemes), part size and structures/attachments.

The high pressure turbine second stage nozzle doublet vane was chosen because it is a static structural component subjected to high temperatures yet it is in a relatively low stress environment. The current state of the art for the nozzle is a multipiece alloy assembly. Individual doublets need to be stress-relieved, brazed, aged and inspected during the manufacturing process, then tack welded and brazed again into the assembly. A benefit from this program would be to reduce manufacturing time and labor. In addition, cooling air to the nozzle may be reduced.

A second component is the high pressure turbine shroud for auxiliary power units (APUs). In this unit, the shroud sees a maximum gas temperature of 1800 °F. The shroud is the most ideal static component as it offers great potential reductions in SFC (e.g., blade tip clearance and weight reduction) life cost, and blade excitation over the current segmented metallic shroud. There has been significant confidence in the design and test of ceramic shrouds with several successful programs, including the Small Heavy Fuel Engine (SHFE) program at Honeywell.

Additive Manufacturing of Polymer Components

In this project, Fused Deposition Modeling (FDM) was used as additive manufacturing technology for fabrication of polymer composites. Different types of materials were used including commercially available polyetherimides—Ultem 9085 and experimental Ultem 1000 mixed with 10 percent chopped carbon fiber. Detailed experimental results of the polymer composite process development and characterization has been described in the second report. In this report, we will describe the testing details of inlet guide vanes fabricated using ABS and carbon fiber reinforced Ultem 1000 and acoustic liners fabricated from Ultem 9085.

Designs for two alternate liner geometries were developed for manufacturing trials. A Helmholtz design similar to the current baseline honeycomb concept and the advanced "Passive-Destructive" liner concept, developed at Honeywell and based on Herschel-Quincke tube theory, were both fabricated for acoustic evaluation. Initial design iterations for both designs were fabricated by Fused Deposition Modeling. FDM process parameters were optimized to print the thinnest acceptable septum walls and best geometric cell shapes for acoustic attenuation and light weight. Two Helmholtz samples were delivered to NASA for acoustic testing. These samples were printed in Ultem 9085, which was chosen as the best alternative material based on the anticipated 250 °F operating temperature of the acoustic liner in engine operation. Figure 6 shows the pictures of the liners and Grazing Flow Impedance Tube test rig at NASA Langley Research Center (LaRC). Details of the test results have been discussed in following sections.

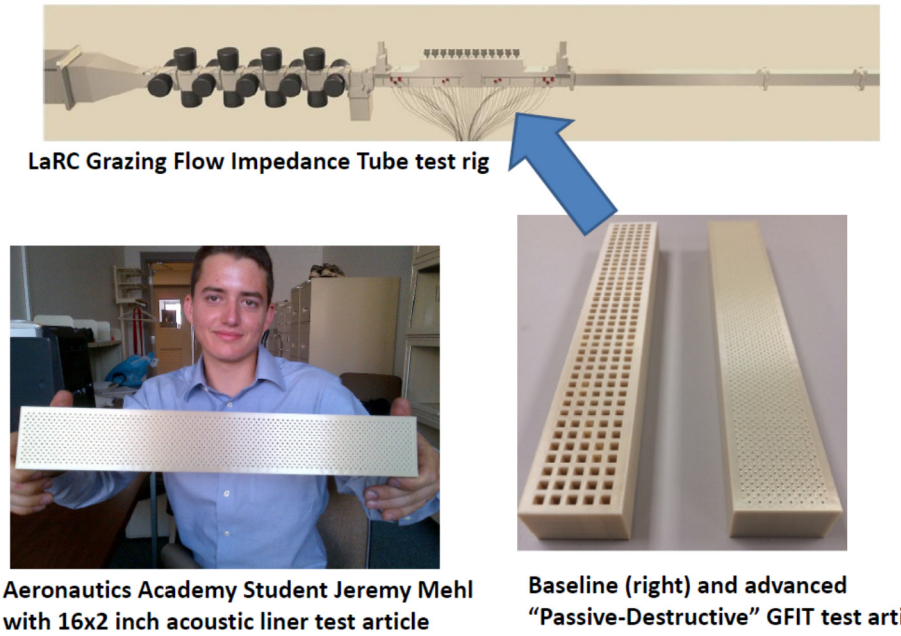

Figure 6.—Noise attenuation of baseline and advanced acoustic liners was evaluated in NASA LaRC grazing flow impedance tube acoustic facility.

Testing of Additively Manufactured Polymer Components

Inlet Guide Vane Cascade Testing

A set of additively manufactured inlet guide vanes were tested in the Engine Research Building (ERB) SW-2 wind tunnel facility as shown in Figures 7(a) and (b). This facility uses the lab-wide central exhaust system to draw atmospheric air through an acrylic wind tunnel. The test section consists of a linear cascade of nine inlet guide vanes spaced 1.5 in. apart. The test area cross-section was 4.5 in. high by 15 in. wide. Flow rate was controlled with a throttling valve downstream of the test section. Inlet flow conditioning tunnel sections were removed for this experiment to allow unobstructed camera views of the test section.

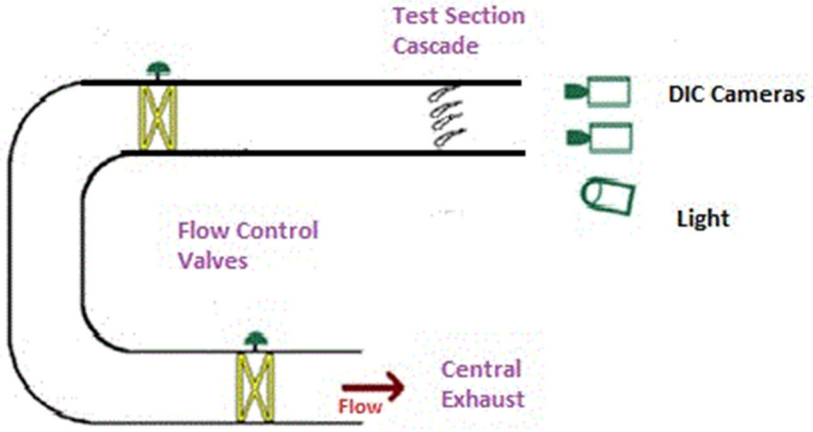

(a)

(b)

Figure 7.—(a) NASA ERB SW-2 general wind tunnel (Schematic). (b) ERB SW-2 facility with IGV cascade and DIC system.

The four different inlet guide vane designs that were tested are shown in Figure 8. Two vanes were made of ABS and two were made of Ultem 1000 with 10 percent chopped carbon fiber. Additionally two fillet designs at the hub and tip of each vane were employed in this test. One set of vanes (ABS and carbon fiber Ultem) was fabricated with the standard Honeywell fillets, while another set of vanes (ABS and Carbon fiber Ultem) was fabricated with a larger reinforced fillet at the tip and hub. The vanes are roughly 6 in. long, with an airfoil section 4.5 in. long. The chord varies from 1.25 to 2 in. All vanes were printed with buildup proceeding from the leading edge to the trailing edge (right to left in the vane configuration shown in Figure 9). Each vane was later painted with a speckled pattern to allow for imaging by the ARAMIS DIC system described below.

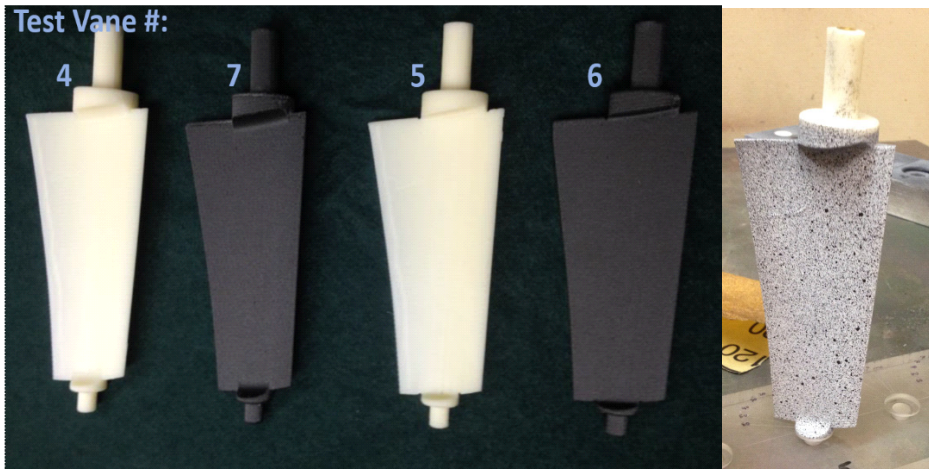

Figure 8.—Inlet guide vanes tested in SW2 cascade.

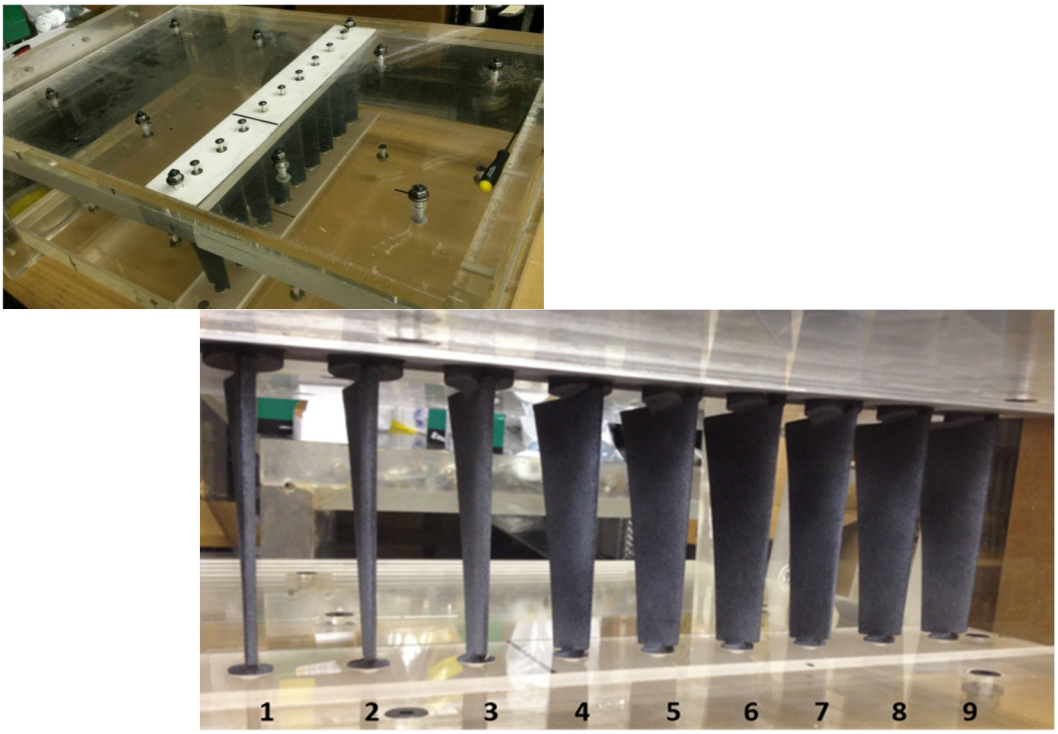

Figure 9.—Inlet guide vane cascade test section.

The individual vanes were mounted in the tunnel ceiling and floor and were secured with a screw through the tunnel ceiling and threaded into the vane stem. The vanes could be rotated and fixed at different angles of incidence. The tunnel inlet was nominally 4.5 by 15 in. The test section included nine vanes total with vanes 4 to 7 being the test articles. The inlet airstream was at room temperature and passed through no flow conditioning sections upstream of the test cascade.

Strain under an aerodynamic load was measured on several vanes using an optical stereoscopic Digital Image Correlation (DIC) technique. All the test vanes were painted with a speckled pattern. The two DIC cameras were placed looking down stream into the tunnel inlet. They were arranged in such a way as to image the pressure face of the four center vanes. The four different test designs were located in this view. Comparison of the speckled patterns of two camera views of the same vane yields the deformation of each vane as it bends under changing loads.

Tests were performed at various inlet velocities ranging from nominally 100 to 600 ft/sec and at angles from 0° to 60°. Additionally the vane cascade was tested in a “closed” position i.e., vanes were set to 90° to the inlet flow in an attempt to fracture the vanes. Deflection up to several millimeters was observed but no fracture was detected, even at the “closed” condition. Deflection and strain data from the DIC system is summarized in Figure 10.

Figure 10 shows typical displacement data acquired from the ARAMIS DIC system. It shows the displacement in the Z (normal to pressure face) direction of the four test vanes at 20°, 30°, 40°, and 50° incidence angle under a 400 ft/sec an airstream. The vanes numbered from left to right are listed in the Table 2. As expected, for all vanes the displacement increases with increasing incidence angle. Also, the largest displacement generally occurs on the ABS vane with the baseline fillet design (vane 5). The vane maximum displacement data for nominal velocities from 100 to 600 ft/sec and 20°, 30°, 40° and 50° angles are summarized in Figure 11. From the graph it is clearly evident that for each angle, the maximum deflection increases with increasing velocity. Also evident, as previously mentioned, the max deflection

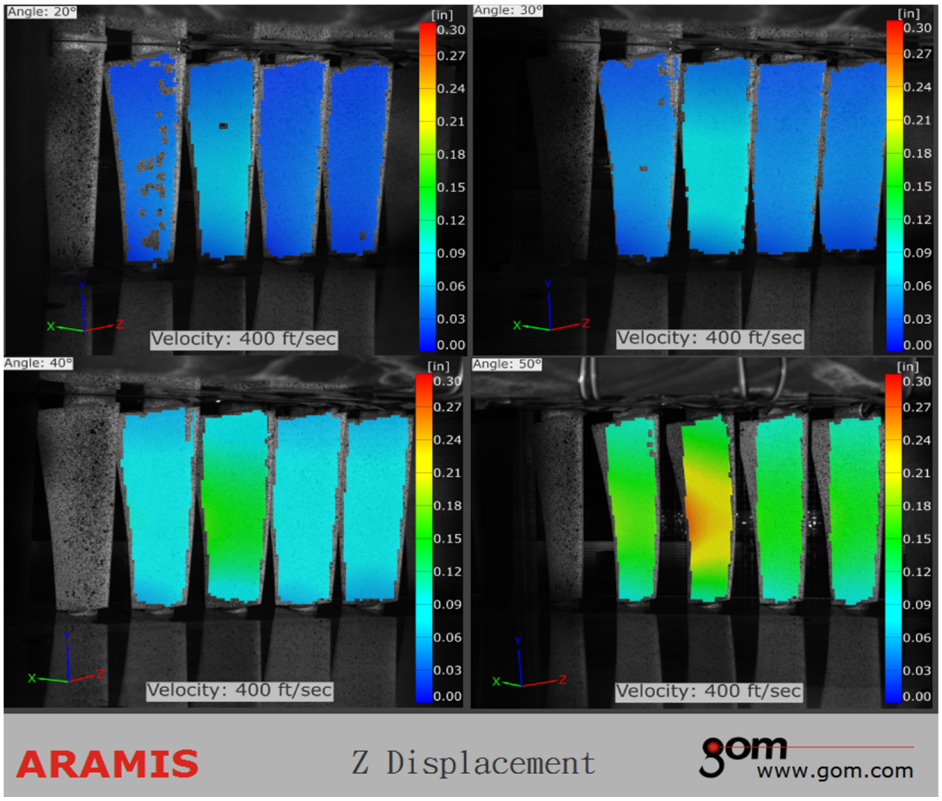

Figure 10.—Displacement in the Z-direction for 20°, 30°, 40° and 50° incidence angle at 400 ft/sec velocity.

TABLE 2.—POSITION OF TEST VANES IN CASCADE

Vane number (left to right)	Material	Fillet design
4	ABS	Reinforced (RP+M)
5	ABS	Baseline (Honeywell)
6	Ultem 1000 w/Carbon	Baseline (Honeywell)
7	Ultem 1000 w/ Carbon	Reinforced (RP+M)

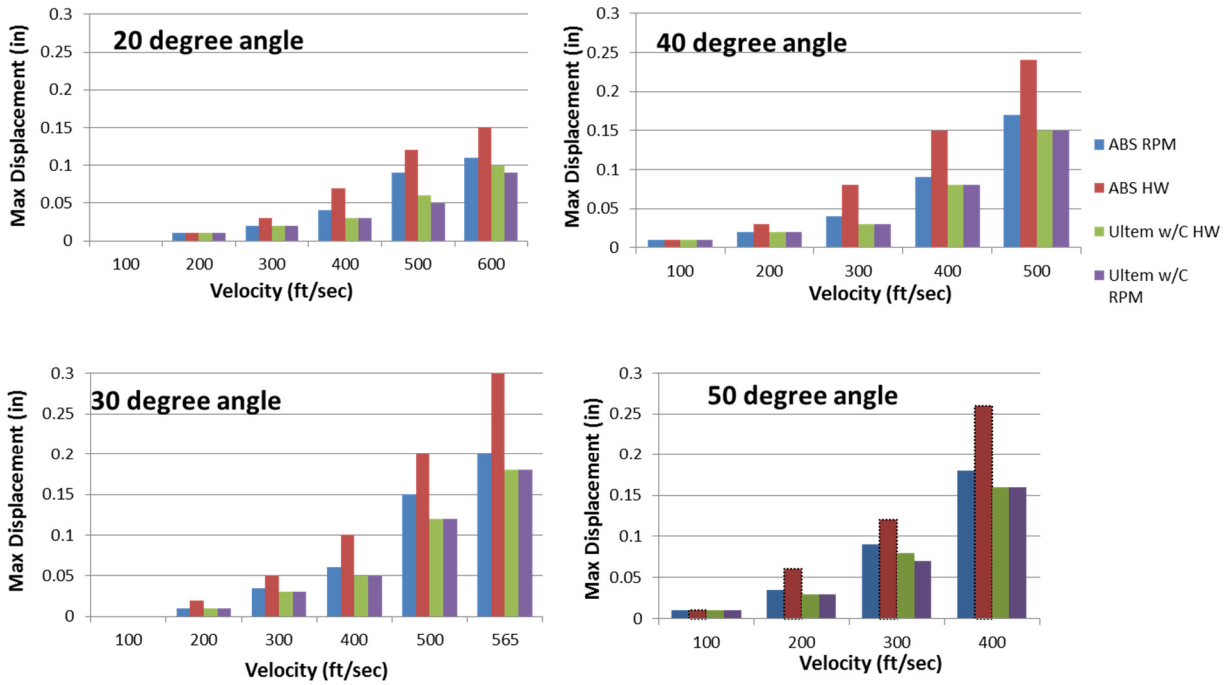

Figure 11.—Displacement data at different velocities and incident angle showing maximum displacement in Z-direction.

increases with increasing incidence angle. Generally the ABS vanes (4 and 5) show higher deflection than the carbon reinforced Ultem 1000 vanes (6 and 7). Additionally this data seems to show that that reinforced fillet improved the stiffness of the vane for the ABS cases but not so much for the Ultem cases. It is important to note however, that these tests were conducted with a very limited number of trials and test specimens and more samples should be tested to confirm this result.

Similarly, Figures 12 and 13 illustrate typical strain data acquired in this test. Figure 12 represents strain in the span wise direction for the four test vanes at 20°, 30°, 40°, and 50° incidence angle under a 400 ft/sec an airstream. Figure 13 shows maximum positive and negative strain in the span wise direction as a function of velocity for the 50° angle case. As with the displacement, the highest strain values were observed on vane 5 (ABS Baseline fillet). The strain values do exhibit a somewhat streaky pattern in all cases. Typically a large negative strain is seen near mid-span of blade and a large positive strain near hub especially at higher angles and speeds. Again, these tests were conducted with a very limited number of runs and test specimens. The main objective was to determine if the vanes would could withstand in air speeds that may be typical of an actual IGV. While a fair amount of bending was observed, none of the four center test vanes fractured during these tests.

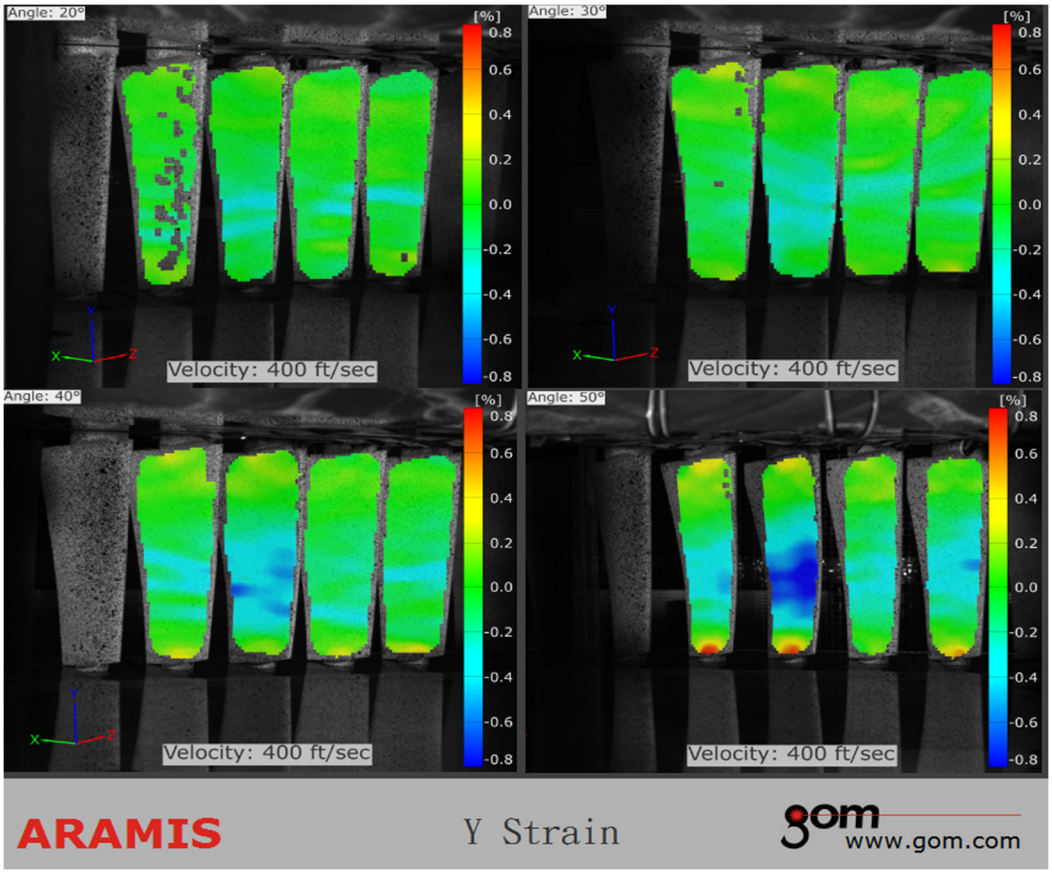

Figure 12.—Strain in the Y-direction for 20°, 30°, 40° and 50° incidence angle at 400 ft/sec velocity.

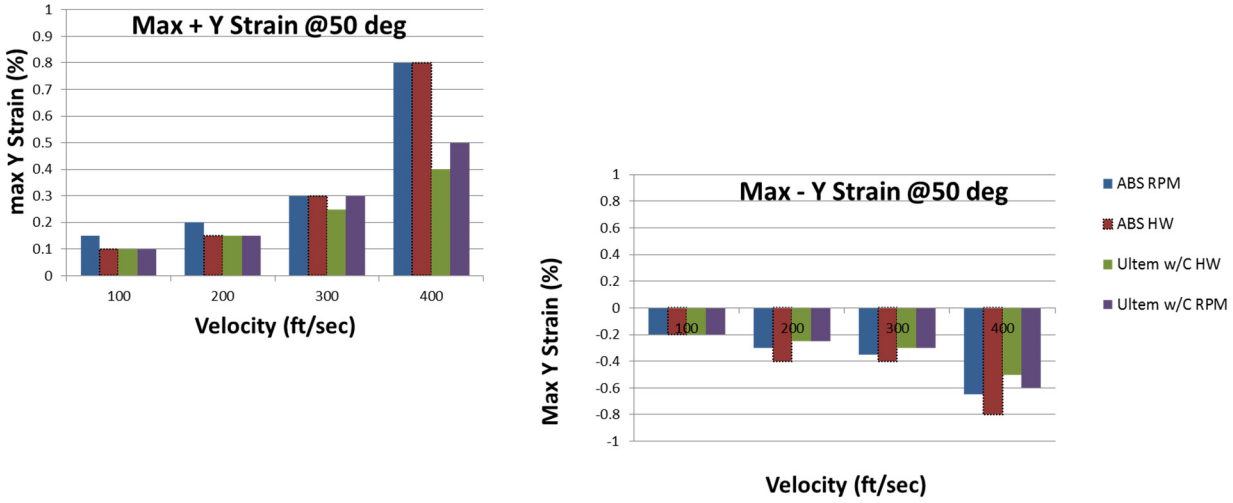

Figure 13.—Maximum strain in Y-direction versus velocity at 50° angle.

Rig Testing of Acoustic Liners

Acoustic liner testing was conducted in the NASA Langley Research Center Grazing Flow Impedance Tube (GFIT) acoustic rig. The measurement process is documented in Reference 3. Acoustic data were collected at three values of flow Mach number and two tone amplitudes. Tones at frequencies of 0.4 to 3.0 kHz in increments of 0.2 kHz were measured. Table 3 provides a summary of the test matrix. The focus of the analysis was on the no flow and the Mach number of 0.3 conditions. Configuration F3 was created at NASA Langley by adding a 3 cgs rayl wire mesh cover sheet to reduce generated flow noise due to the size of the surface openings.

Typical measurement results are shown in Figure 14 for the conventional construction liner for a tone source level of 120 dB with no flow. Comparable data is available for all of the conditions summarized in Table 3. The graph shows the changes in tone amplitude from the upstream to the downstream end of the liner sample. The significant change in the tone amplitude occurs at frequencies of 1.4 and 1.6 kHz corresponding to the resonant frequency of this locally-reacting liner.

A rough estimate of the insertion loss for each liner sample can be made by subtracting the sound level at 40 in. from the sound level at 0 in. Figure 15 shows the results of that calculation for the no flow and Mach number of 0.3 cases at 120 dB tone level. The results at 140 dB are similar.

TABLE 3.—CONFIGURATIONS TESTED AT THE NASA LANGLEY GRAZING FLOW IMPEDANCE TEST FACILITY

Configuration	Liner	Mach = 0.0		Mach = 0.3		Mach = 0.5	
		120 dB	140 dB	120 dB	140 dB	120 dB	140 dB
1	Conventional construction	X	X	X	X	X	X
2	Fused deposition model	X	X	X	X	X	X
3	Advanced concept	X	X	X	X	X	X
F3	Advanced concept w/linear facesheet	X	X	X	X	X	--

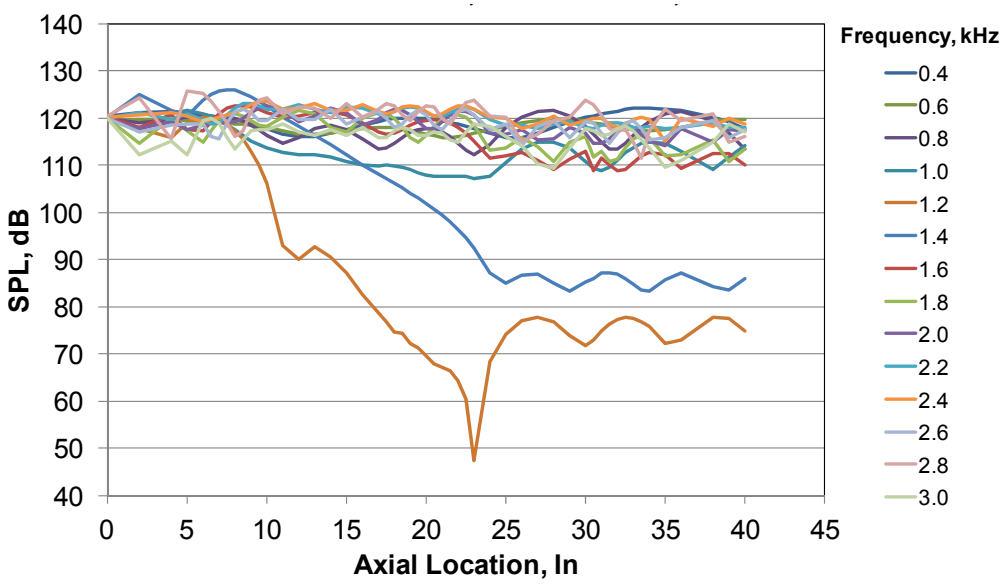

Figure 14.—Measured sound levels of the conventional acoustic liner.

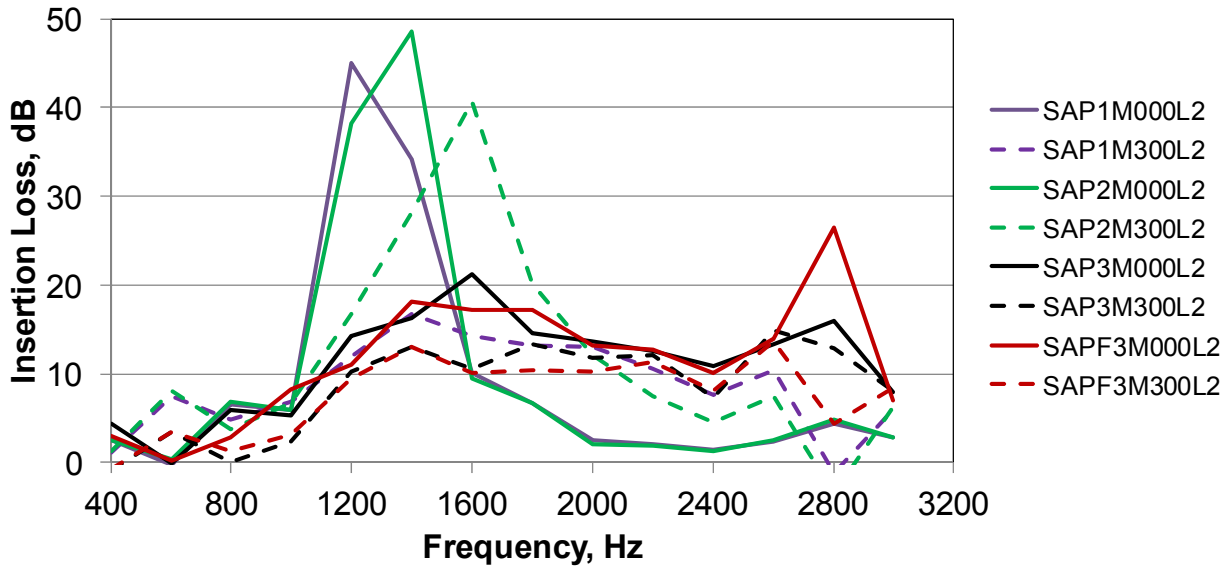

Key:

SAP1M000L2 = Configuration 1, Mach = 0.0
SAP1M300L2 = Configuration 1, Mach = 0.3
SAP2M000L2 = Configuration 2, Mach = 0.0
SAP2M300L2 = Configuration 2, Mach = 0.3
SAP3M000L2 = Configuration 3, Mach = 0.0
SAP3M300L2 = Configuration 3, Mach = 0.3
SAPF3M000L2 = Configuration F3, Mach = 0.0
SAPF3M300L2 = Configuration F3, Mach = 0.3

Figure 15.—Insertion loss of all liner samples estimated from the GFIT measurements.

For the no flow case (solid lines in Fig. 15), the resonance frequencies of the conventional construction (Configuration 1) and the Fused Deposition Model (Configuration 2) are comparable. The frequency of the Fused Deposition Model is slightly higher (of the order of 100 Hz), indicating that the average chamber height of the liner may be slightly shorter than the conventional construction liner. The advanced concept liner data (Configuration 3 and F3) do not show evidence of a resonant frequency as expected. The advanced concept liner insertion loss in the range of 1600 to 3000 Hz shows improved higher frequency attenuation per the design intent.

The Mach 0.3 data (dotted lines in Fig. 15) show that the flow effect on the liner samples differ. The flow had minimal effect on the performance of the advanced concept liners. However, the flow effect had a significant effect on the performance of the conventional liner samples. The conventional construction liner lost its resonance behavior, but the Fused Deposition Model liner maintained a resonant behavior, but it shifted to a higher frequency. The flow also improved the attenuation of the conventional liners from 1800 to 2600 Hz, eliminating the benefit of the advance liner construction.

The acoustic impedance of the four liner samples was educed following the process in Reference 3. Figure 16 shows the results for the two locally-reacting liner configurations. Also shown on the figure are the results from the DC flow measurements reported in Reference 2. As expected, the GFIT measured resistance of the conventional construction liner matched the DC Flow results reasonably well. However, the resistance of the Fused Deposition Model liner with flow was noticeably less than the conventional construction liner. This result explains the insertion loss results in Figure 15. Lower resistance due to flow results in lower high frequency attenuation and maintains the resonant characteristic of the liner. It is likely that the hole diameter of the Fused Deposition Model liner was larger than the conventional construction liner. Measurements are planned to verify the diameter of the holes in the two liners.

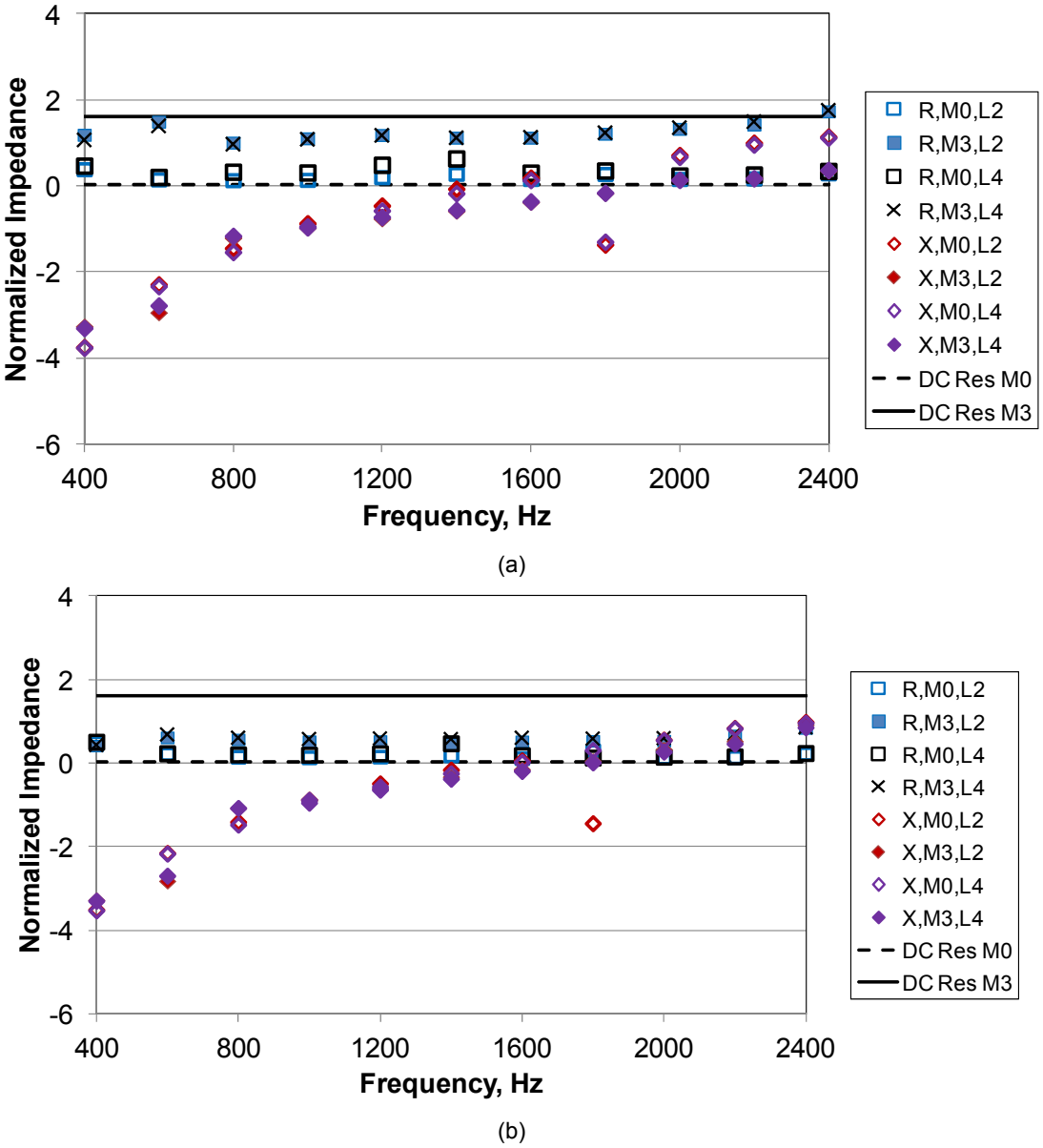

Key:	
R,M0,L2 = Resistance, Mach = 0.0, SPL = 120 dB	X,M0,L2 = Reactance, Mach = 0.0, SPL = 120 dB
R,M3,L2 = Resistance, Mach = 0.3, SPL = 120 dB	X,M3,L2 = Reactance, Mach = 0.3, SPL = 120 dB
R,M0,L4 = Resistance, Mach = 0.0, SPL = 140 dB	X,M0,L4 = Reactance, Mach = 0.0, SPL = 140 dB
R,M3,L4 = Resistance, Mach = 0.3, SPL = 140 dB	X,M3,L4 = Reactance, Mach = 0.3, SPL = 140 dB
DC Res M0 = Resistance at Mach = 0.0, Ref. 7	DC Res M3 = Resistance at Mach = 0.3, Ref XX1

Figure 16.—Acoustic impedance of the conventional liner as educed from the GFIT measurements. (a) Conventional construction. (b) FDM liner.

Figure 17 shows the results for the two passive-destructive liner concepts. First, it is noted that the liner resistance is higher than for the locally reacting configurations with no flow. This higher resistance leads to the improved broadband performance at the no flow condition. Further, it can be seen that the advanced liner shows minimal change in resistance with flow. Since the resistance of the advanced liner is comparable to the resistance of the conventional liner at Mach 0.3, it is expected that acoustic performance of the two liners will be similar. Further optimization of the advance liner concept is needed to exploit the characteristics that were identified in this study.

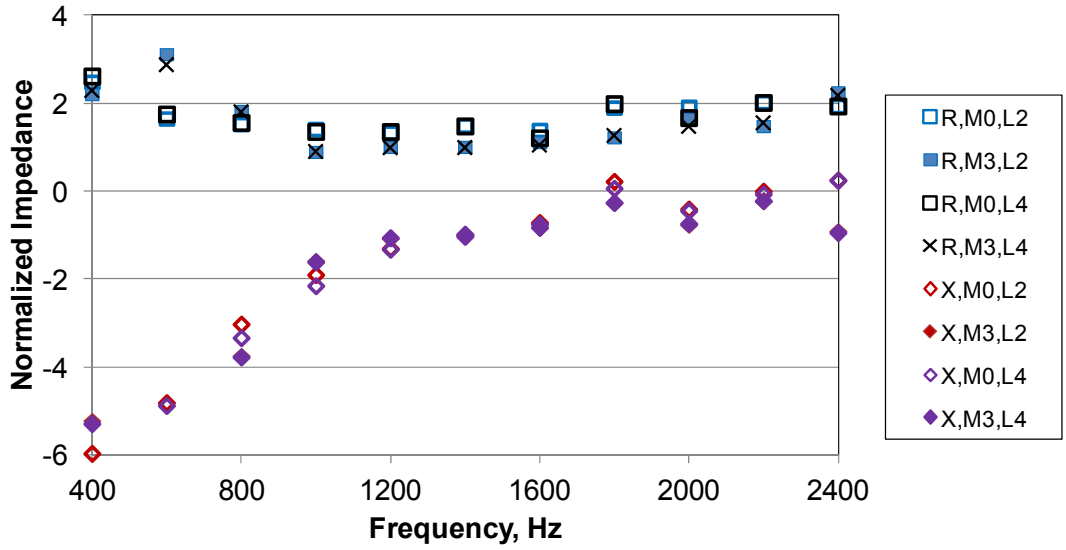

(a)

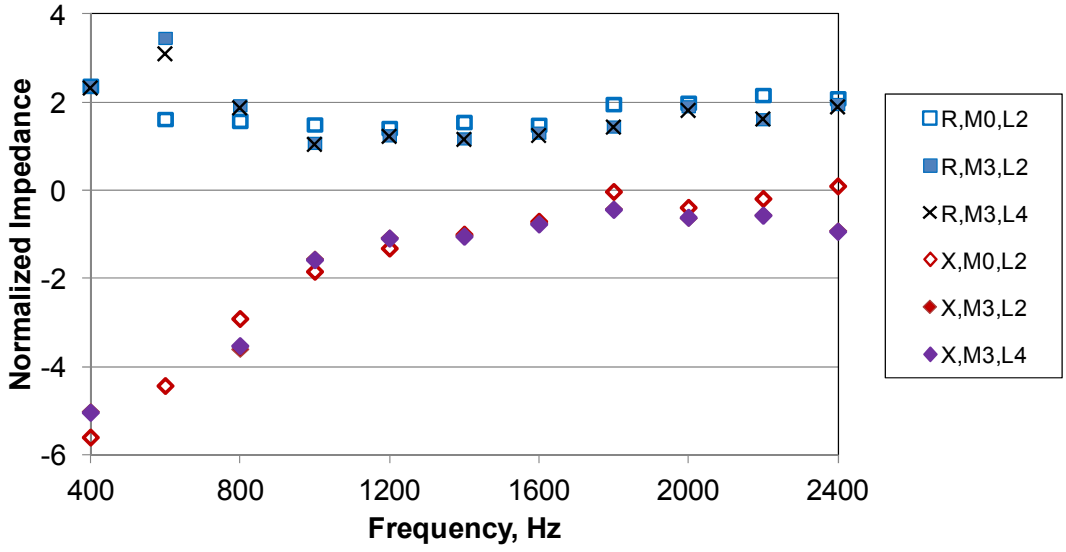

(b)

Key:

R,M0,L2 = Resistance, Mach = 0.0, SPL = 120 dB	X,M0,L2 = Reactance, Mach = 0.0, SPL = 120 dB
R,M3,L2 = Resistance, Mach = 0.3, SPL = 120 dB	X,M3,L2 = Reactance, Mach = 0.3, SPL = 120 dB
R,M0,L4 = Resistance, Mach = 0.0, SPL = 140 dB	X,M0,L4 = Reactance, Mach = 0.0, SPL = 140 dB
R,M3,L4 = Resistance, Mach = 0.3, SPL = 140 dB	X,M3,L4 = Reactance, Mach = 0.3, SPL = 140 dB

Figure 17.—Acoustic impedance of the advanced concept liner as educed from the GFIT measurements. (a) As fabricated. (b) With linear facesheet.

Summary and Conclusions

System analysis studies indicate that there are potential fuel saving benefits from PMC and CMC engine components for a regional-jet class system. The CMC components were combustor liner, the high-pressure and low-pressure turbine blade/vanes, and the core nozzle. The benefits included a weight reduction in the aforementioned components due to replacing metallic parts with ceramic-based alternatives, in addition to the elimination of requisite turbine cooling. The PMCs were applied in the inlet acoustic liner, the fan stator and the first four rows of the high-pressure compressor vanes and the PMC benefits consisted of weight reductions only in each component. The resultant propulsion system generated a 4.9 percent fuel burn improvement over the baseline and a 7.7 percent increase in landing-takeoff (LTO NO_X) margin with respect to the CAEP/6 stringency.

In case of polymer composites, two types of acoustic liners were fabricated from Ultem 9085 polymer and tested in rigs. They included a Helmholtz design similar to the current baseline honeycomb concept and the advanced "Passive-Destructive" liner concept, developed at Honeywell and based on Herschel-Quincke tube theory. Compressor inlet guide vanes, fabricated from ABS and carbon fiber reinforced Ultem 1000, were tested in wind tunnel to measure the deflection and strain. The ABS vanes show higher deflection than the carbon reinforced Ultem 1000 vanes. Additionally this data seems to show that reinforced fillet improved the stiffness of the vane for the ABS but not so much for the Ultem 1000. Detailed analysis of results for polymer and ceramic composites are presented in second and third part of the report.

References

1. M.C. Halbig, M.H. Jaskowiak, J.D. Kiser, and D. Zhu, "Evaluation of Ceramic Matrix Composite Technology for Aircraft Turbine Engine Applications," 51st AIAA Aerospace Sciences Meeting including the New Horizons Forum and Aerospace Exposition, 07–10 January 2013, Grapevine (Dallas/Ft. Worth Region), Texas.
2. R.W. Claus, A.L. Evans, J.K. Lytle and L.D. Nichols, "Numerical Propulsion System Simulation," *Computing Systems in Engineering*, Vol. 2, No. 4, pp.357–364, 1991.
3. NPSS User Guide Software Release: NPSS_1.6.5.
4. NPSS Reference Sheets Software Release: NPSS_1.6.5.
5. M.R. Kirby and D.N. Mavris, "The Environmental Design Space," 26th Congress of International Council of the Aeronautical Sciences (ICAS), Anchorage, Alaska, Sept 14–19, 2008, ICAS 2008-4.7.3.
6. Asif A. Syed, et al, "The Steady Flow Resistance of Perforated Sheet Materials in High Speed Grazing Flows, NASA/CR—2002-211749, July 2002.
7. M.G. Jones, et al., "Comparative Study of Impedance Education Methods, Part 2: NASA Tests and Methodology." AIAA-2013-2125, 19th AIAA/CEAS Aeroacoustics Conference, May 27–29, 2013, Berlin, Germany.